Acta Materialia 123 (2017) 90–101

Contents lists available at ScienceDirect

Acta Materialia

journal homepage: www.elsevier.com/locate/actamat

Full length article

Atomic scale processes of phase transformations in nanocrystalline NiTi shape-memory alloys

Won-Seok Ko [a, b, *], Sascha B. Maisel [b], Blazej Grabowski [b], Jong Bae Jeon [c], Jörg Neugebauer [b]

[a] School of Materials Science and Engineering, University of Ulsan, Ulsan 44610, Republic of Korea
[b] Max-Planck-Institut für Eisenforschung GmbH, Max-Planck-Str. 1, 40237 Düsseldorf, Germany
[c] Functional Components and Materials R&D Group, Korea Institute of Industrial Technology (KITECH), Busan 618-230, Republic of Korea

ARTICLE INFO

Article history:
Received 6 August 2016
Received in revised form
30 September 2016
Accepted 7 October 2016
Available online 24 October 2016

Keywords:
Shape-memory alloy
Nickel-titanium
Nanocrystalline material
Phase transformation
Molecular dynamics simulation

ABSTRACT

Molecular dynamics simulations are performed to investigate temperature- and stress-induced phase transformations in nanocrystalline nickel-titanium shape-memory alloys. Our results provide detailed insights into the origins of the experimentally reported characteristics of phase transformations at the nanoscale, such as the decrease of the transformation temperature with grain size and the disappearance of the plateau in the stress-strain response. The relevant atomic scale processes, such as nucleation, growth, and twinning are analyzed and explained. We suggest that a single, unified mechanism—dominated by the contribution of a local transformation strain—explains the characteristics of both temperature- and stress-induced phase transformations in nanocrystalline nickel-titanium.
© 2016 Acta Materialia Inc. Published by Elsevier Ltd. This is an open access article under the CC BY-NC-ND license (http://creativecommons.org/licenses/by-nc-nd/4.0/).

1. Introduction

Shape-memory alloys have been widely used for many applications utilizing their unique properties of shape-memory behavior and superelasticity. Among the various shape-memory alloys discovered so far, nickel-titanium (NiTi) shape-memory alloys with equiatomic or nearly equiatomic compositions have received great attention owing to their excellent mechanical properties, biocompatibility, corrosion resistance, and their ability to transform close to room temperature [1]. In NiTi alloys, the reversible temperature- and stress-induced phase transformation between B2 austenite and B19′ martensite results in the shape-memory effect and in superelasticity, respectively [1].

Recently, nanocrystalline NiTi shape-memory alloys have attracted special attention because of their excellent strength, thermomechanical cyclic stability, linear superelasticity, and the large temperature window for superelasticity [2–5]. Because these exceptional properties are likely related to unique characteristics of phase transformations at the nanoscale, experimental studies on phase transformations in nanocrystalline NiTi are ongoing [2–8]. A noticeable characteristic of nanocrystalline NiTi is an over-stabilization of the austenite phase with respect to the martensite phase. In the case of the temperature-induced phase transformation, it has been reported that the transformation temperature decreases with decreasing grain size and that the transformation to martensite is completely suppressed below a critical grain size [9–11]. In the case of the stress-induced phase transformation, a steep hardening in the stress-strain response has been reported for nanocrystalline NiTi, while polycrystalline NiTi with larger grains shows a clear plateau in the stress-strain curve [2–4]. Consequently, the transformation in nanocrystalline NiTi occurs at higher stress levels, indicating again an over-stabilization of the austenite phase [2–4].

This over-stabilization of the austenite phase has not only been reported for nanocrystalline materials, but also for shape-memory nanoparticles with different boundary conditions, such as free standing particles or nanoparticles embedded in bulk metallic glass [11]. It is reasonable to expect that the fundamental mechanism underlying phase transformations at the nanoscale differs from its bulk counterpart. Several candidate mechanisms have been proposed to explain the over-stabilization of the austenite phase. The first one is the "*interfacial energy contribution mechanism*" [11–13]

* Corresponding author. School of Materials Science and Engineering, University of Ulsan, Ulsan 44610, Republic of Korea.
E-mail address: wonsko@ulsan.ac.kr (W.-S. Ko).

http://dx.doi.org/10.1016/j.actamat.2016.10.019
1359-6454/© 2016 Acta Materialia Inc. Published by Elsevier Ltd. This is an open access article under the CC BY-NC-ND license (http://creativecommons.org/licenses/by-nc-nd/4.0/).

which promotes the relative difference between the interfacial energy of the austenite and martensite phase. For example, if the grain boundary energy of the austenite phase is lower than that of the martensite phase, a decrease in the transformation temperature is expected with smaller grain size. The second one is the "*internal defect contribution mechanism*" [11,14] which promotes the role of internal defects, e.g., dislocations, as heterogeneous nucleation sites. Based on the assumption that a larger grain or particle contains more internal defects than a smaller one, the suppression of the martensitic phase transformation is expected with smaller grain or particle size. The final mechanism is the "*strain-contribution mechanism*" [4,10,11] which promotes a mechanical constraint by the presence of interfaces. Following this idea, the phase transformation is suppressed with smaller grain or particle size, because the increased transformation strain energy due to the strong mechanical constraint can contribute to an increase in the free energy.

Among these mechanisms, the strain-contribution mechanism has been supported by a recent experiment on the stress-induced phase transformation in nanocrystalline NiTi alloys [4]. The experiment reported X-ray diffraction profiles recorded during *in situ* tensile loading and unloading. The results indicate a gradual degeneration of the diffraction profiles from a multiple-peaks mode to a continuous, single-peak mode with decreasing grain size. This is an indicator of lattice strains inside the transformed structure due to strong mechanical constraints by grain boundaries.

However, several uncertainties remain, which have so far prohibited the conclusion that the strain-contribution mechanism indeed governs phase transformations in nanocrystalline NiTi. Most notably, the experiment in Ref. [4] presented only limited information on the microstructure during the phase transformation. Generally, it is known that the evolution of the microstructure—especially the twinning behavior—is critical for phase transformations in shape-memory alloys [1], but the twinning in nanocrystalline NiTi and its role during the phase transformation are still uncertain. Further, it is questionable whether a single, unified mechanism governs both temperature- and stress-induced phase transformations. Contrary to experiments on the stress-induced phase transformation, experiments on the temperature-induced phase transformation of nanocrystalline materials are rather challenging and generally limited because of the following difficulties: The temperature-induced phase transformation of nanocrystalline NiTi usually involves the formation of an interfering intermediate R-phase during cooling induced by the presence of metastable Ni_4Ti_3 precipitates [1,7–9]. Moreover, the availability of *in situ* experiments is greatly limited because the transformation temperature of nanocrystalline NiTi can approach 0 K, limiting experimental capabilities [11].

In order to overcome these difficulties and to supplement experiment, theoretical approaches by means of mesoscale [15] and atomistic simulations are useful. Especially, molecular dynamics (MD) simulations combined with semi-empirical interatomic potentials can enable a detailed understanding of the underlying mechanisms. For example, MD simulations have been successfully used to elucidate the deformation behavior of metallic nanocrystalline materials [16–18] and phase transformations of shape-memory alloys [19–22]. As for the phase transformations in nanocrystalline shape-memory alloys, there has been a recent MD simulation work [23] focusing on a related shape-memory alloy system (NiAl). However, because the work in Ref. [23] was based on an interatomic potential which predicts a wrong martensite structure as compared to experiment [23,24], the respective conclusions are rather limited.

In the present study, we have investigated phase transformations in nanocrystalline NiTi shape-memory alloys based on a recently developed interatomic potential [22] that correctly reproduces the experimentally reported phase transformation between B2 austenite and B19′ martensite. We present MD simulation results that are consistent with available experimental information. Based on the results we are able to shed light on the atomistic processes involved during the phase transformations, such as nucleation and growth, the twinning behavior, and the occurrence of an irrecoverable strain. The governing mechanism of temperature- and stress-induced phase transformations in nanocrystalline alloys is critically discussed by confronting the proposed mechanisms with our simulation results and available experimental data.

2. Methodology

The MD simulations were performed based on the second nearest neighbor modified embedded-atom method (2NN MEAM) with an interatomic potential specifically designed for the Ni–Ti binary system [22]. This potential was developed with the aim to accurately reproduce the temperature- and stress-induced phase transformations in equiatomic NiTi. It reproduces the phase transformation between the B2 austenite and B19′ martensite phase as well as the fundamental physical properties (structural, thermodynamic, and defect properties) of the relevant intermetallic compounds and solid solutions. All of the present simulations were performed with a radial cutoff distance of 5.0 Å, which is larger than the second nearest-neighbor distance of B2 NiTi. A detailed formulation of the 2NN MEAM formalism is available in the literature [25–27].

Nanocrystalline cells were generated using the Voronoi construction method [28] with random positions and crystallographic orientations for each grain. Initially, cube-shaped cells with the B2 structure were generated considering designated average grain sizes. Most of the cells were composed of 30 grains, but the cell with the largest average grain size (30 nm) was generated with only 5 grains to render the computations feasible. The resulting average grain diameter (D), number of grains, cell dimensions, and number of atoms for each cell are summarized in Table 1.

A series of MD simulations was then performed using the LAMMPS code [29] with a time step of 2 fs. The Nosé-Hoover thermostat [30,31] and the Parrinello-Rahman barostat [32] were used for controlling temperature and pressure, respectively. Periodic boundary conditions were applied along all three dimensions to remove spurious surface effects. During the simulations, cell dimensions, cell angles, and individual atomic positions were allowed to fully relax. Initially, the generated cells were subjected to an energy minimization process using the conjugate gradient method to avoid unstable atomic positions near the generated grain boundary configurations. Annealing at 400 K, i.e., above the austenite finish (A_f) temperature, was applied to recover the initial B2 austenite structure.

The temperature-induced phase transformation was investigated by performing MD simulations in an isobaric-isothermal (*NPT*) ensemble at zero-pressure. From the initial temperature of 400 K, the temperature was gradually decreased to 10 K and increased again to 400 K with cooling and heating rates of ±0.5 K/ps. During the simulations, atomic volumes at the specific temperature and their changes were recorded to observe the occurrence of phase transformations.

The stress-induced phase transformation was likewise investigated with MD simulations in an *NPT* ensemble. Prior to loading, zero-stress transformation temperatures for each nanocrystalline cell were obtained from simulation results of the temperature-induced phase transformation. The A_f temperature of every nanocrystalline cell turned out to be lower than 400 K. Knowing this result, the temperature was kept at 400 K to maintain the B2

Table 1
Average grain diameter (D), number of grains, cell dimensions, and number of atoms in the nanocrystalline cells considered in the present MD simulations.

D (nm)	4	8	12	16	20	30
Number of grains	30	30	30	30	30	5
Cell dimensions (nm)	$10 \times 10 \times 10$	$20 \times 20 \times 20$	$30 \times 30 \times 30$	$40 \times 40 \times 40$	$50 \times 50 \times 50$	$41 \times 41 \times 41$
Number of atoms	71692	577873	1976336	4679243	9134320	5159445

austenite phase in its zero-stress state. A strain-controlled uniaxial tensile loading was then applied by controlling the cell dimensions which corresponds to the loading direction with a strain rate of 5×10^8 s^{-1} and maximum strain of 8%. The strain rate of the present MD simulations is in the conventional range of usual MD simulations ($10^7 \sim 10^9$ s^{-1}) [33], but it is orders of magnitude higher than that of usual experiments ($10^{-5} \sim 10^{-1}$ s^{-1}[3]). To analyze the effect of the strain rate, additional simulations were performed for the simulation cell with a grain size of 8 nm using strain rates of 5×10^7, 1×10^8, 2×10^8, 1×10^9, and 2×10^9 s^{-1}. When the strain reached the maximum value of 8%, cells were unloaded to recover their original shape. During the simulations, pressures in the directions orthogonal to the tensile axis were set to 0 and the cell angle between those directions was allowed to relax, leading to a dynamic response to the tensile strain.

In order to visualize the evolution of the microstructure during the phase transformations, local atomic arrangements were identified using a common neighbor analysis (CNA) [34,35] as implemented in the OVITO program [36]. Although the CNA algorithm was initially not developed to differentiate between the B2 austenite and B19′ martensite phases, we confirmed that it is nevertheless well suited for that purpose. Only directly at the grain boundaries, a small fraction of the transformed phase was not properly recognized due to residual strains, making the grain boundaries appear slightly thicker after the transformation. In the CNA pattern, atoms depicted in blue represent the B2 austenite phase, while red atoms represent the B19′ martensite phase. Grain and domain boundary regions are shown in gray. To visualize local plastic deformation, the von-Mises local shear invariant [37] of each atom was calculated and visualized using the OVITO program [36].

The virtual diffraction method developed by Coleman et al. [38,39] was utilized to investigate the simulated phase transformations on an equal footing with experimental data. The method generated 2θ X-ray line profiles using a three-dimensional reciprocal lattice mesh with a spacing of 0.005 Å. The radiation source imitated Cu K_α X-rays ($\lambda = 1.54178$ Å). The range of 2θ was restricted to $35^\circ < 2\theta < 55^\circ$, since profiles of the B19′ martensite phase are known to show three peaks at 38.18°, 43.65° and 44.78° associated with the (110), (020), and (111) planes, respectively [4,40]. In this range, the B2 austenite phase indicates a single peak at 42.24° associated with the (110) plane [4]. All line profiles were created using an optimal 2θ bin size of 0.075° determined by several trials.

3. Results

3.1. Temperature-induced phase transformation in nanocrystalline NiTi alloys

Fig. 1 shows the temperature dependence of the atomic volume during cooling and reheating of nanocrystalline NiTi for various grain sizes. As the initial B2 austenite phase is cooled down (blue curves), it transforms for most grain sizes into the B19′ martensite phase with a positive volume change as expected from an experimental work [41] and previous MD simulations [22]. The discontinuous jump in the atomic volume represents the phase transformation event, and the corresponding temperature is recorded as the martensite start temperature (M_s). Fig. 2 shows representative atomic snapshots for the initial state (400 K; top row) and after cooling (10 K; middle row). At the initial temperature of 400 K, nanocrystalline NiTi consists of austenite grains separated by grain boundaries as indicated by the blue and gray color, obtained from a common neighbor analysis [34,35]. During the cooling process, the austenite phase mostly transforms into martensite as indicated by the red color in the middle row. Simulation cells with grain sizes larger than 8 nm show a clear martensitic transformation, while the one with a grain size of 4 nm does not show any discontinuous volume change (Fig. 1) indicating the absence of a phase transformation. The cell with a grain size of 8 nm shows an intermediate transformation behavior with a significant fraction of retained austenite. The overall increase of the volume with decreasing grain size (as most evident for the 4 and 8 nm case in Fig. 1) scales with the number of grain boundary atoms due to a positive access volume of the grain boundaries.

The occurrence of a martensitic phase transformation is further confirmed by the virtual diffraction method [38,39]. The left panel of Fig. 3 shows X-ray diffraction profiles of nanocrystalline NiTi for the various grain sizes at 400 K (red curves) and 10 K (blue). As the B2 austenite phase is stabilized for all grain sizes at 400 K, the profiles consistently indicate a single peak around 42–43°. After decreasing the temperature to 10 K, most profiles change, with the changes depending on the grain size. In nanocrystalline NiTi with larger grain sizes (12, 16, and 20 nm), the profiles indicate three peaks, demonstrating the formation of the B19′ martensite phase. For the cell with a grain size of 8 nm, the peaks gradually merge into a single broad peak at slightly higher 2θ values. For the cell with a grain size of 4 nm, the change in the diffraction profile is negligible because the phase transformation is suppressed.

Upon reheating, the B19′ martensite phase transforms back into the B2 austenite phase at a higher temperature than the M_s temperature, again being accompanied by a discontinuous jump in the volume as shown in Fig. 1 (red curves). This temperature is recorded as the austenite finish (A_f) temperature. We observe a complete match between the atomic volume dependence during cooling and reheating, if the temperature is higher than the A_f temperature. This result implies that the B2 austenite phase is completely recovered after the reheating process. The complete recovery of the austenite phase is also confirmed by the atomic configurations in Fig. 2 (lowest panel) and by results of the virtual diffraction method (not shown) which indicate the recovery of a single peak in the diffraction profiles. Fig. 4 summarizes the grain size dependence of the M_s and A_f temperatures of the temperature-induced phase transformation. The result clearly indicates a decrease in both transformation temperatures as the grain size decreases, which is in agreement with experimental works [9–11].

Fig. 5 shows a detailed view of the microstructure evolution during the martensitic transformation for the simulation cell with a grain size of 30 nm. At the initial temperature of 400 K, the sample consists of the B2 austenite phase and grain boundaries [Fig. 5(a)]. After cooling, the austenite phase transforms into the B19′ martensite phase leaving the grain boundaries mostly unaffected [Fig. 5(b)]. However, we observe the formation of a new kind of boundary inside the enlarged grain (“Grain 2”) which needs to be

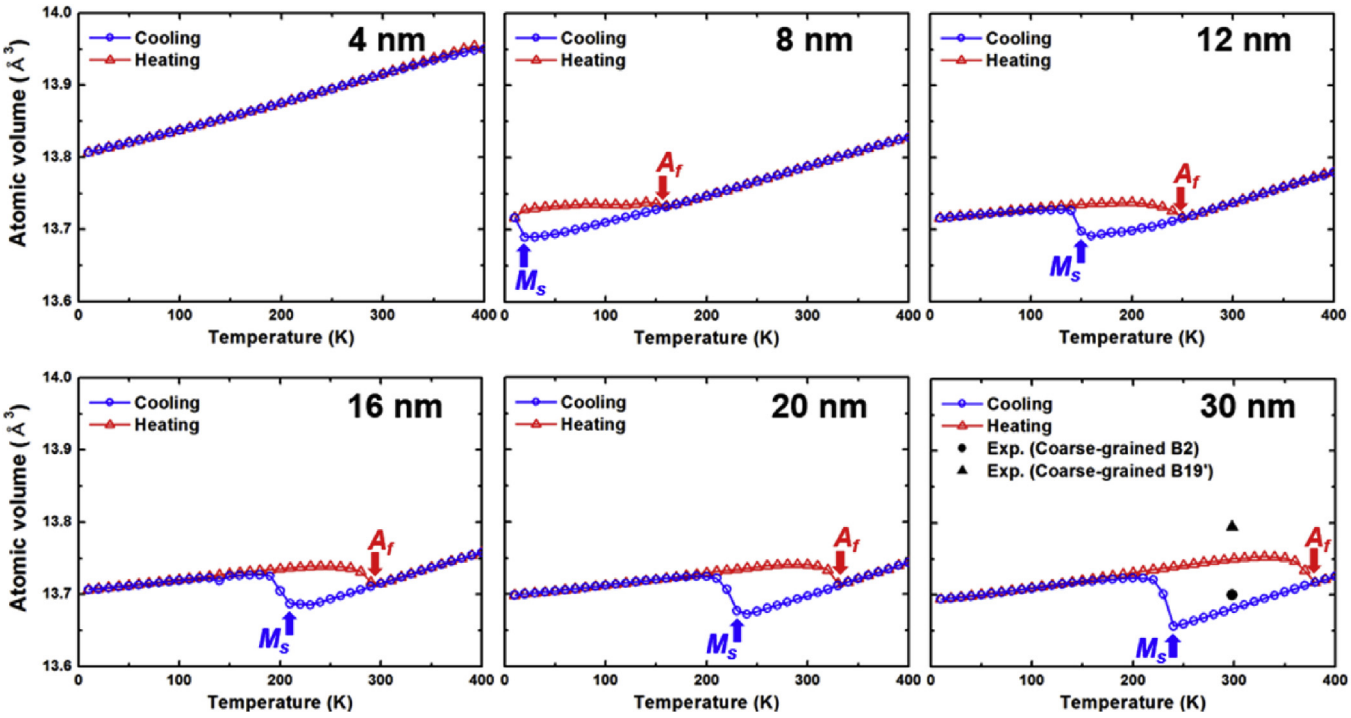

Fig. 1. Atomic volume dependence of nanocrystalline NiTi during cooling and reheating for various average grain sizes as indicated in each plot. The discrete jumps represent the occurrence of the martensitic phase transformation. The martensite start (M_s) and the austenite finish (A_f) temperature are indicated by the blue and red arrow, respectively. (For interpretation of the references to colour in this figure legend, the reader is referred to the web version of this article.)

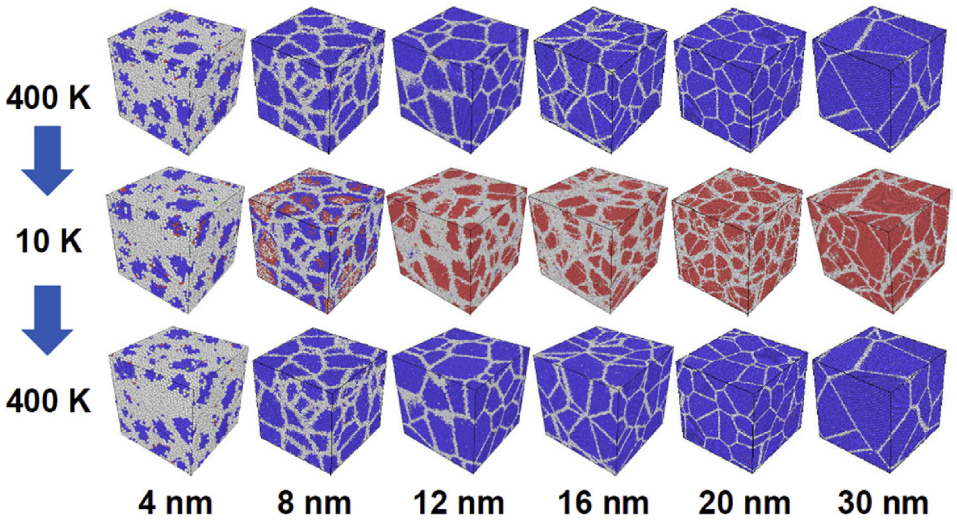

Fig. 2. Atomic configurations of nanocrystalline NiTi with various average grain sizes at the initial state (400 K), after cooling (10 K) and after reheating (400 K). The color of the atoms is scaled according to the CNA pattern. In each snapshot, blue atoms correspond to the B2 austenite structure, red atoms to the B19′ martensite structure, and gray atoms to the grain and domain boundaries. (For interpretation of the references to colour in this figure legend, the reader is referred to the web version of this article.)

distinguished from the original grain boundary. It is a domain boundary that separates multiple domains inside of a single martensite grain, and it disappears after reheating into the austenite phase as we have explicitly confirmed (not shown). The domain structure is emphasized in Fig. 5(c) by a different color code revealing an interesting substructure. Each domain consists of twinned B19′ martensite variants with finely dispersed (001) compound twin boundaries. A similar martensite structure was reported in a previous experiment on NiTi nano-particles inside of bulk metallic glass and it was referred to as a “herringbone” structure [42].

Fig. 6 shows representative snapshots of the cooling and reheating process at various temperatures, enabling the detection of nucleation and growth events. During the cooling process, the martensite phase nucleates at the grains' interior as visible for the configurations at 240 and 230 K. As the temperature is further decreased, the martensite phase grows towards the grain boundaries forming multiple domains inside of each grain. The nucleation and growth of the austenite phase during reheating strictly differs from the nucleation and growth of the martensite phase during

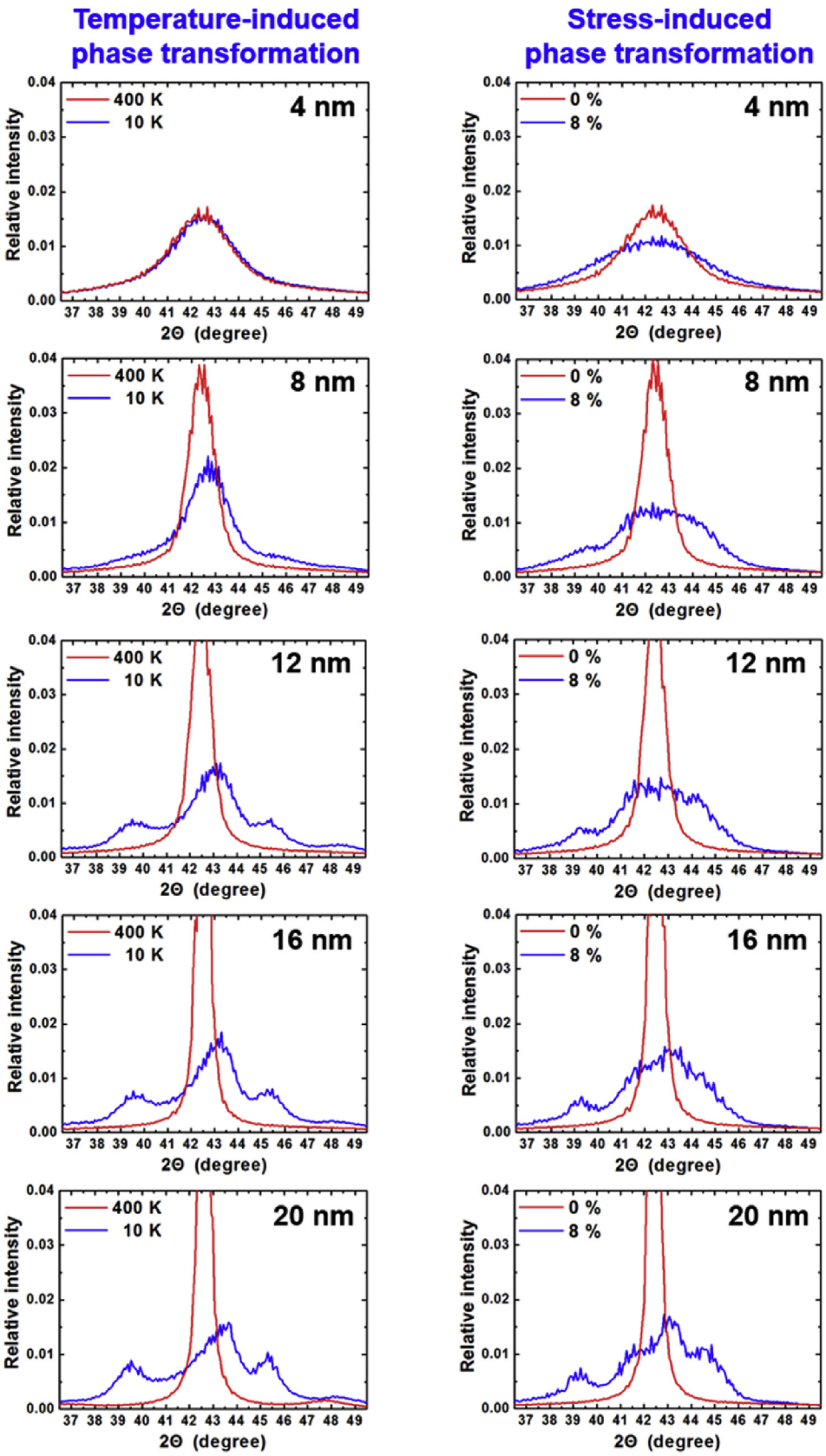

Fig. 3. X-ray diffraction profiles of nanocrystalline NiTi with various average grain sizes obtained by the virtual diffraction method [38,39]. The profiles were recorded at 400 K and 10 K during the temperature-induced transformation and at strains of 0% and 8% during the stress-induced transformation.

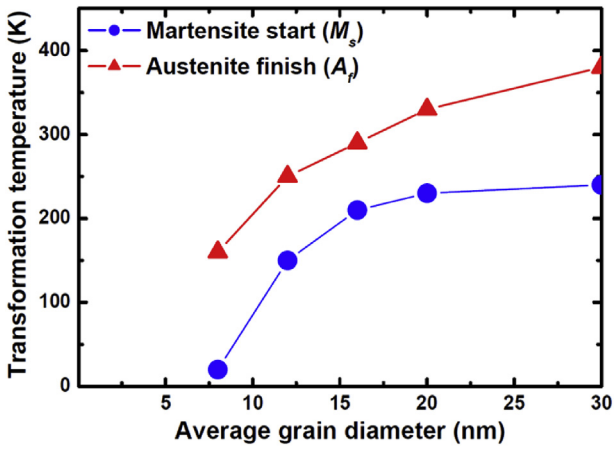

Fig. 4. Size dependence of the martensite start (M_s) and austenite finish (A_f) temperature of nanocrystalline NiTi obtained from the cooling and reheating processes shown in Fig. 1.

cooling. The austenite phase nucleates at the grain and domain boundaries as visible for the configurations at 250 K and 310 K, and not in the grains' interior as found for the martensite phase. Upon a further temperature increase, the austenite phase grows towards the grains' interior and the martensite phase disappears.

3.2. Stress-induced phase transformation in nanocrystalline NiTi alloys

Fig. 7 shows the stress-strain response of nanocrystalline NiTi for various grain sizes. Unlike most conventional alloys, shape-memory alloys exhibit a sigmoidal (i.e., S-shaped) stress-strain behavior because of the stress-induced phase transformation. As the tensile loading is applied to the B2 austenite phase, it transforms into the B19′ martensite phase showing a plateau in the curve. During unloading, the martensite phase transforms back into the austenite phase showing the plateau at a lower stress level. The resultant stress-strain curve indicates a hysteresis loop. Compared to previous experiments [2–4], a significant overshooting of the stress levels is revealed by the simulations (theoretical stresses: ≈2 GPa and experimental ones: ≈0.5 GPa). A similar behavior was reported in a previous MD simulation on nanocrystalline Al [33] and explained by the extremely high strain rate of usual MD simulations [33]. The present MD simulations also reveal a strong dependency of the stress level on the strain rate as shown in Fig. 8(a). If an extrapolation is performed using the present MD data down to lower strain rates, the resultant stress is in a range of the experimental data as shown in Fig. 8(b).

Fig. 9 shows representative atomic configurations at different strain levels: initial state (0%), maximum tensile loading (8%), and after unloading (0%). Simulation cells with grain sizes 8 nm and larger clearly undergo a martensitic transformation contrary to the results for the temperature-induced phase transformation, where the transformation was significantly suppressed for the 8 nm grain sized material. In fact, for the strain induced transformation even the cell with the smallest grain size (4 nm) shows a certain fraction of transformed grains, which was not the case for the temperature induced transformation. However, under strain the martensitic transformation is incomplete: In all simulation cells a substantial amount of retained austenite (blue color) can be observed at the maximum loading condition, even for the largest grain size (30 nm). This fact is quantified in Fig. 10 by the open red triangles showing that the fraction of retained austenite is about 10% with

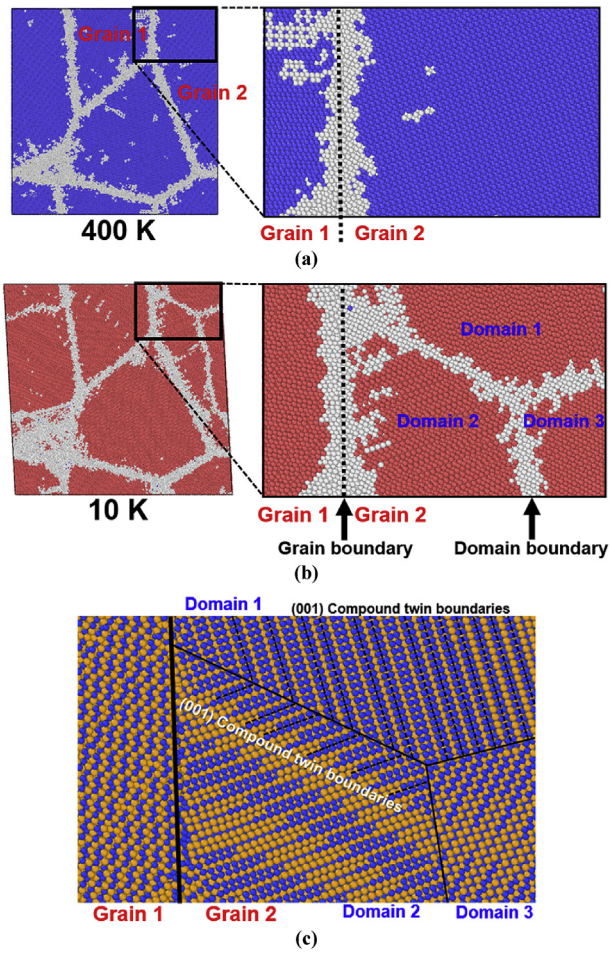

Fig. 5. Atomic configurations of nanocrystalline NiTi with an average grain size of 30 nm (a) before (400 K) and (b) after (10 K) the cooling process. The color of the atoms is scaled according to the CNA pattern. Blue atoms correspond to the B2 austenite structure, red atoms to the B19′ martensite structure and gray atoms to grain and domain boundaries. A part of the cross section is magnified to illustrate internal structures of a grain before and after the martensitic transformation. (c) Visualization of the domain and twin structures after the martensitic transformation. Ni and Ti atoms are represented by blue (dark gray) and orange (gray) balls, respectively. In domain 1, (001) compound twin boundaries orthogonal to the page are fully indicated. Twin boundaries in domain 2 are partially indicated because they are not orthogonal to the page. Twin boundaries in domain 3 are not indicated because they are parallel to the page. (For interpretation of the references to colour in this figure legend, the reader is referred to the web version of this article.)

only statistical variations as a function of grain size. The retained austenite can be explained by the presence of preferentially and non-preferentially oriented grains in the stress-induced phase transformation as the loading direction breaks the original (on-average) symmetry in contrast to temperature which acts isotropically, leaving no retained austenite for larger grain sizes (filled red triangles in Fig. 10).

X-ray diffraction profiles corresponding to 0% and 8% tensile strain are shown in the right panel of Fig. 3. As all simulation cells are composed of the B2 austenite phase at 0% strain, the profiles indicate a single peak around 42–43°. At the maximum strain of 8%, the profiles change indicating the occurrence of the phase transformation. In the cells with larger grain sizes, multiple peaks are visible indicating the formation of the B19′ martensite phase. The peaks are not as pronounced as for the temperature induced transformation, due to the above mentioned incomplete transformation. As the grain size decreases, the peaks gradually merge

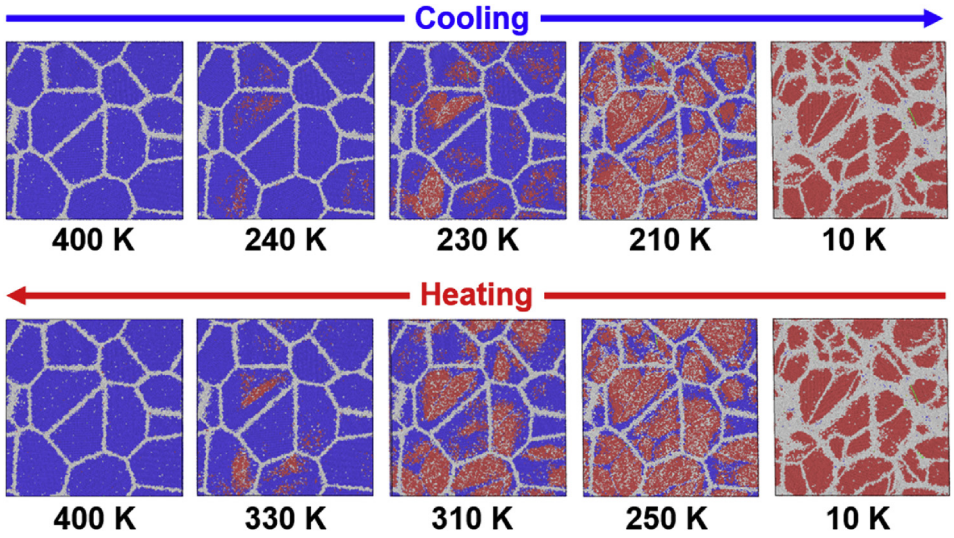

Fig. 6. Atomic configurations of nanocrystalline NiTi with an average grain size of 20 nm during the cooling the reheating process. The color of the atoms is scaled according to the CNA pattern. In each snapshot, blue atoms correspond to the B2 austenite structure, red atoms to the B19′ martensite structure and gray atoms to grain and domain boundaries. (For interpretation of the references to colour in this figure legend, the reader is referred to the web version of this article.)

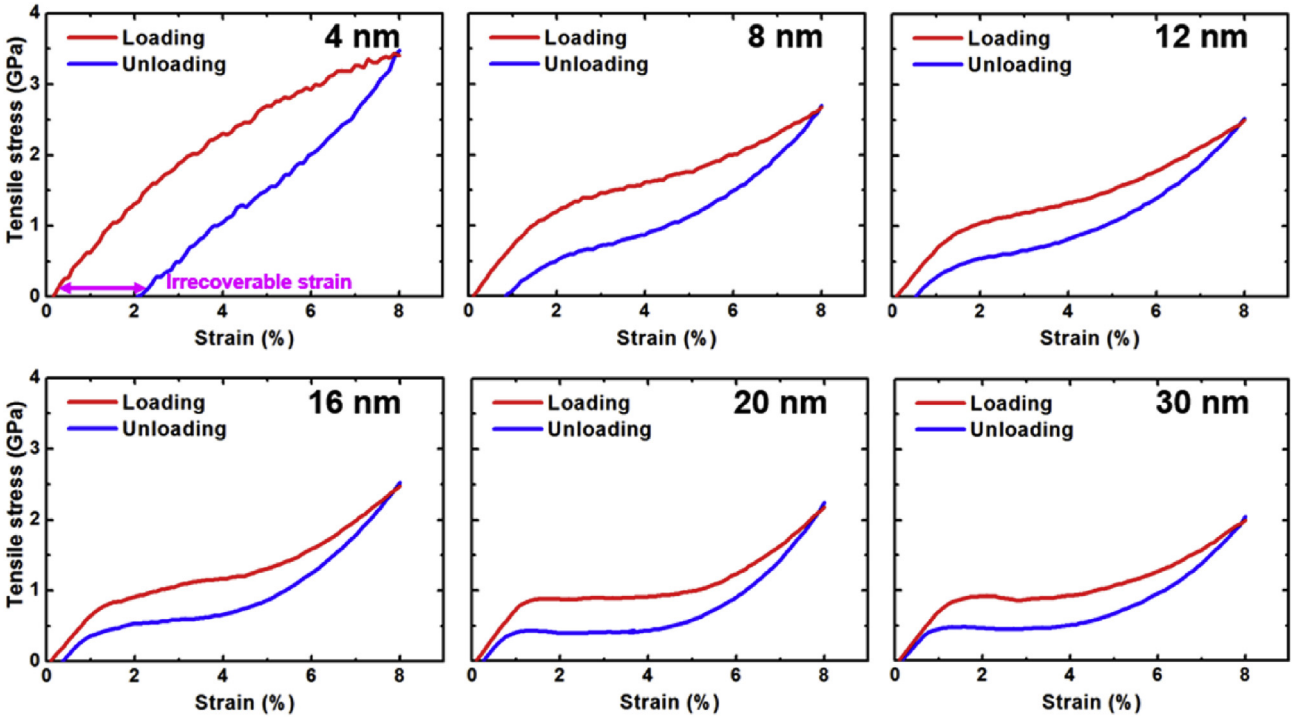

Fig. 7. Stress-strain response of nanocrystalline NiTi with various average grain sizes under tensile loading and unloading at 400 K.

into a single broad peak, which is however different from the peak of the B2 austenite phase due to the fact that there is always a certain fraction of transformed grains. The results are in general agreement with a previous experimental study [4] which also presented a single broad peak in the stress-induced phase transformation of nanocrystalline NiTi with very small grain sizes (10 nm).

Fig. 11 shows snapshots of atomic configurations during the tensile loading and unloading process at several strain levels. Generally, nucleation and growth proceeds as in the case of the temperature-induced transformation. The martensite phase nucleates at the grains' interior and grows towards the grain boundaries during the loading process, and the austenite phase nucleates at the grain and domain boundaries and grows towards the grains' interior during the unloading process. The herringbone structure with multiple martensite domains is also observed after the austenite-to-martensite transformation.

4. Analysis of the stress-strain response: irrecoverable strain and how to mitigate it

By comparing the different stress-strain curves (Fig. 7) we can

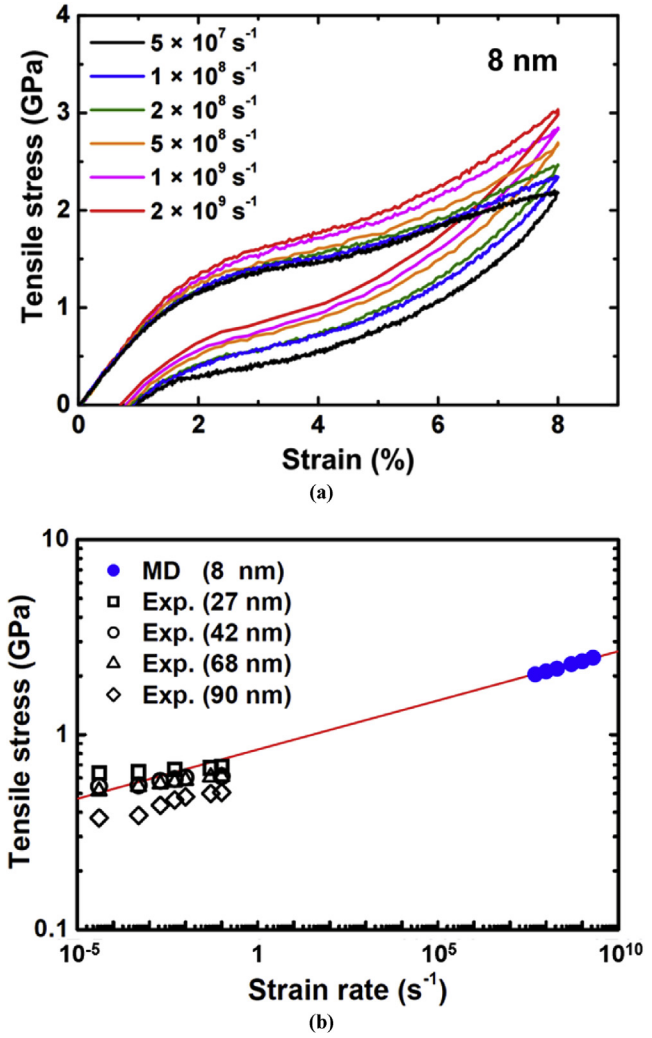

Fig. 8. (a) Stress-strain response of nanocrystalline NiTi with an average grain size of 8 nm under various strain rates at 400 K. (b) Tensile stresses (σ) at 7% strain during the loading process under various strain rates ($\dot{\varepsilon}$) as recorded from the present MD simulations [Fig. 8(a)] and from a previous experiment [3]. The extrapolation (red solid line) is based on a power fitting function [$\sigma = a(\dot{\varepsilon}/\dot{\varepsilon}_0)^b$ with $a = 0.8384$ GPa, $b = 0.0504$, and $\dot{\varepsilon}_0 = 1\text{s}^{-1}$] and uses as input only the MD data (blue points). (For interpretation of the references to colour in this figure legend, the reader is referred to the web version of this article.)

observe the following two important trends. First, the overall stress increases as the grain size decreases which is consistent with the usual grain boundary strengthening or Hall-Petch behavior. This finding implies that the overall deformation is governed by the deformation of the grains' interior rather than that of the grain boundaries such as grain boundary sliding. Second, the plateau gradually disappears as the grain size decreases indicating a hardening in the stress-strain response. These are general characteristics of the stress-induced phase transformation in nanocrystalline NiTi, and the present results agree well with previous experiments [2–4] as quantified in Fig. 12. The figure compares our results with experimental data [2–4] in terms of the plateau ($\sigma_h - \sigma_l$) which we have defined as shown in Fig. 12(a). While there is an overshooting of the stress levels due to the above discussed strain rate dependence, the general characteristics of the experimental data are successfully reproduced. For example, both results indicate the hardening [increase in σ_h; Fig. 12(c)] and the disappearance of the plateau [increase in $\sigma_h - \sigma_l$; Fig. 12(d)] with decreasing grain size.

However, there appears to be an inconsistency between the present simulations and experiments regarding the amount of the hysteresis. Whereas the experiments [2–4] reported a narrow hysteresis, the simulations indicate a large hysteresis (hysteresis loop area) in nanocrystalline NiTi with smaller grain sizes. We have found that the inconsistency is caused by the occurrence of an irrecoverable strain (remnant strain after unloading, i.e., at zero external stress) in the present simulations. Fig. 7 shows that the irrecoverable strain is more severe in simulation cells with smaller grains and that it correlates with the amount of the hysteresis. One possible explanation of this irrecoverable strain would be that a certain fraction of retained martensite remains after the unloading process, either caused by an insufficient relaxation time or by a too low temperature. However, as indicated in Fig. 9 the martensite phase is hardly observed after the unloading process. We further confirmed that the irrecoverable strain does not disappear after a separated annealing simulation at 800 K with an annealing time of 200 ps.

The other possible explanation of the irrecoverable strain is that plastic deformation has occurred inside the grains or at the grain boundaries. In fact, plastic deformation at the grain boundaries is a more likely explanation since we observe that the irrecoverable strain strongly increases with decreasing grain size. To examine this possibility, we have investigated the atomic local shear strains after the unloading process for each of the simulation cells. Our results (Fig. 13) clearly indicate that the plastic deformation is localized at the grain boundaries. As the grain boundary area occupies a significant fraction of the small grain-sized material, the irrecoverable strain is more severe. We expect that this localized plastic deformation is related to the metastability of the original grain boundary structures of the nanocrystalline cells prepared initially with the austenite phase in the “as-cast state”. Because the nanocrystalline cells are mainly connected by random high-angle grain boundaries, the atomic structure in the grain boundary regions is very complex with many local energetic minima. The irrecoverable strain and resulting large hysteresis can be explained by a process of approaching a more stable state of the grain boundary regions under application of the tensile stress.

Irrecoverable strain is generally problematic and unwanted in applications of shape-memory alloys, since it strongly limits the efficiency of the shape-memory effect. We have therefore investigated ways to mitigate it and we found that a pre-training of the material utilizing cyclic loading is very useful. Pre-training is generally utilized for the stabilization of the hysteretic response of shape-memory alloys before their final application [43,44]. Fig. 14 shows a typical stress-strain response before (light green curves) and after several loading cycles (blue curves). The plastic deformation at the grain boundaries, the irrecoverable strain, and the resultant hysteresis in the stress-strain response are significantly reduced by the pre-training. In fact, already after the first cyclic loading most of the irrecoverable strain is removed, as shown by the thin gray lines. Incidentally, the experiments which reported a narrow hysteresis for small grain sizes [2–4] were based on nanocrystalline NiTi which had undergone a pre-training of several loading cycles. Thus, comparing experiment and our simulations under the same conditions (i.e., after pre-training) the apparent inconsistency disappears.

5. Analysis of the mechanism governing phase transformations in nanocrystalline NiTi

The good agreement of the present simulation results with available experimental data provides confidence that the underlying mechanism is captured by the simulations. Next, we will

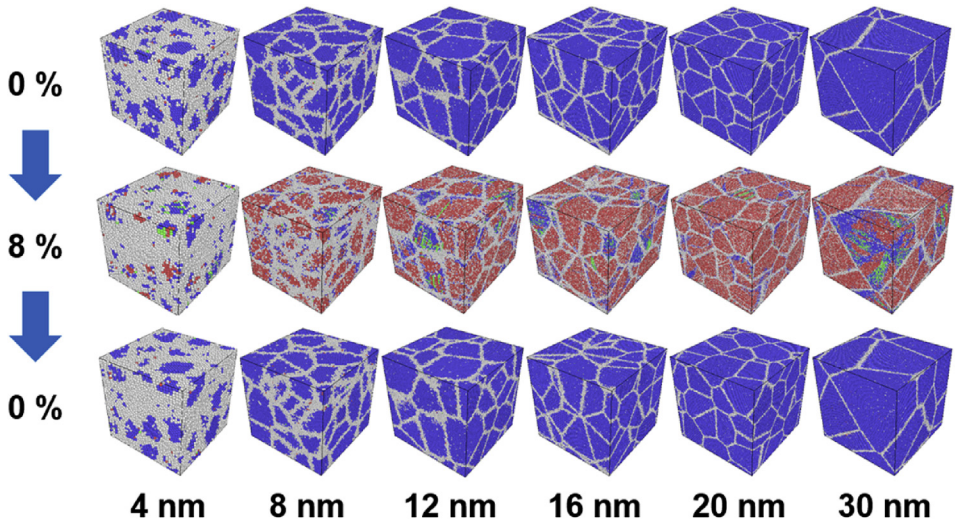

Fig. 9. Atomic configurations of nanocrystalline NiTi at the initial state (0% strain), after the maximum tensile loading (8% strain) and after the unloading (0% strain) process at 400 K. The color of the atoms is scaled according to the CNA pattern. In each snapshot, blue atoms correspond to the B2 austenite structure, red atoms to the B19′ martensite structure and gray atoms to grain and domain boundaries. (For interpretation of the references to colour in this figure legend, the reader is referred to the web version of this article.)

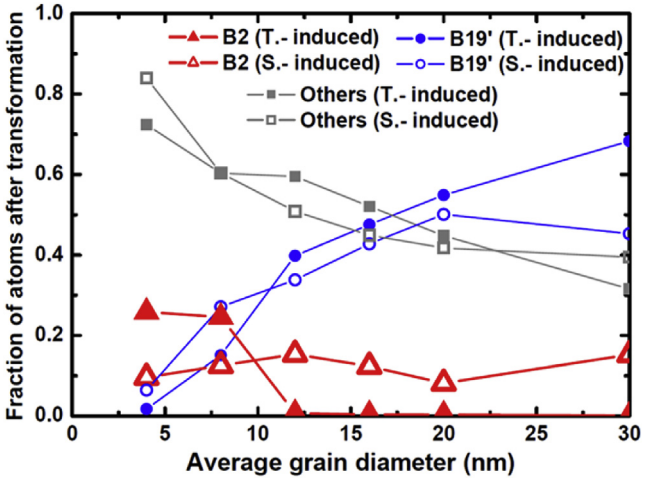

Fig. 10. Fractions of the B2 austenite and B19′ martensite phases after the temperature- and stress-induced phase transformation obtained by analyzing local environments of each atom according to the CNA pattern. “Others” indicates fractions of atoms belonging to grain and domain boundaries and atoms distorted from the austenite and martensite positions due to thermal noise.

confront the three, previously proposed mechanisms (see Sec. 1) with our results, in order to reveal the most probable mechanism, governing temperature- and stress-induced phase transformations in nanocrystalline NiTi alloys.

The present results raise an objection to the validity of the *internal defect contribution mechanism* as a main mechanism. Although all of our MD simulations have been performed without any internal defects (e.g., Frank-Read sources) except for grain boundaries, the experimentally observed characteristics of the phase transformations are correctly reproduced.

The *interfacial energy contribution mechanism* is apparently consistent with experimental observations. This mechanism is based on the assumption that the grain boundary energy of the austenite phase is lower than that of the martensite phase. Since a large fraction of atoms in nanocrystalline NiTi with small grain sizes belongs to grain boundaries, the austenite phase (including its grain boundaries) is thermodynamically stabilized over the martensite phase (including its grain boundaries). Therefore, a decrease in the transformation temperatures and an increase in the transformation stresses can be expected with smaller grain size. A recent phase field study [15] reproduced successfully several of the reported characteristics of phase transformations in nanocrystalline NiTi by assuming that the austenite grain boundaries are more stable than the ones of martensite. However, the interfacial energy contribution mechanism cannot by itself explain the nucleation and growth processes along with the decrease in the M_s temperature, which follow from our simulations. At the M_s temperature, the nucleation of the martensite phase predominantly starts in the grains' interior (Figs. 6 and 11). This means that nucleation and growth of the martensite phase cannot be solely caused by the difference in the grain boundary energy of austenite and martensite. The phase field modeling in Ref. [15] in fact revealed that the martensitic transformation is indirectly affected by the grain boundary energy difference. The latter induces retained austenite regions at the grain boundaries which in turn cause substantial strain gradients penetrating into the grains' interior. The strain gradients are critical for the suppression of the martensitic transformation and for the specific domain formation as also observed in our study.

The most probable mechanism is the *strain contribution mechanism*, explaining well all present simulation results as well as the experimental data. This mechanism successfully explains the asymmetric nucleation and growth behavior between the austenite-to-martensite and the martensite-to-austenite transformation as well as the over-stabilization of the austenite phase. Because the nanocrystalline NiTi samples of the present simulations and the corresponding experiments [2–8] are initially prepared with the austenite phase in the “as-cast state” (strain-free state), the austenite-to-martensite transformation is a process to alter the initial shape of the austenite grains. During the transformation, the heterogeneous nucleation of the martensite phase directly at grain boundaries is suppressed because it would result in an accumulation of local strains, due to the vicinity of the grain boundaries. Thus, the martensite nucleation is constrained to the grains' interior and this constraint is more severe in smaller grain sized cells, which explains the decrease of the transformation

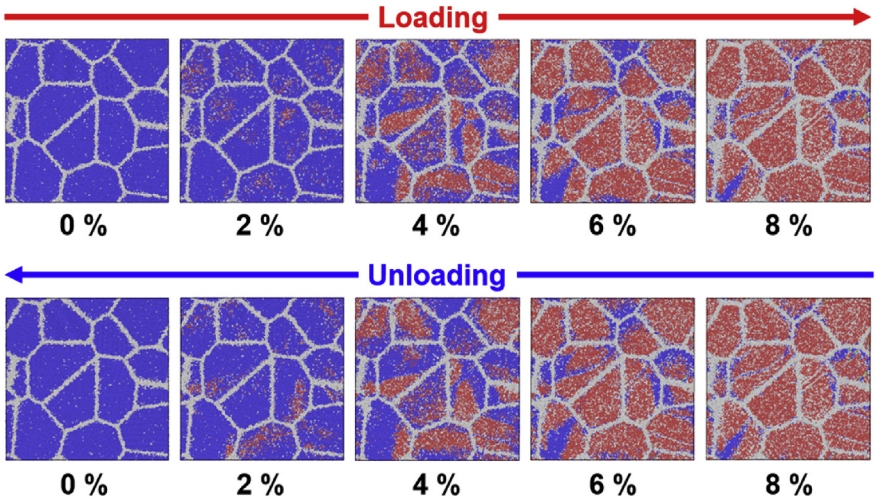

Fig. 11. Atomic configurations of nanocrystalline NiTi with an average grain size of 20 nm during tensile loading and unloading at 400 K. The color of the atoms is scaled according to the CNA pattern. In each snapshot, blue atoms correspond to the B2 austenite structure, red atoms to the B19′ martensite structure and gray atoms to grain and domain boundaries. (For interpretation of the references to colour in this figure legend, the reader is referred to the web version of this article.)

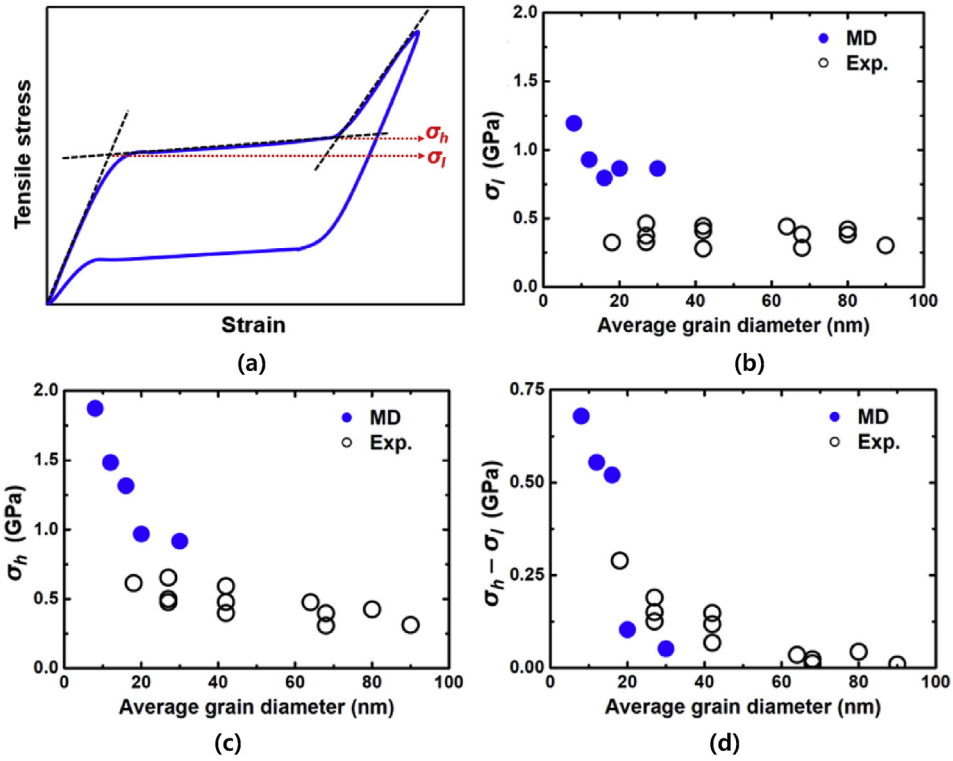

Fig. 12. (a) Schematic illustration of the process to quantify the plateau ($\sigma_h - \sigma_l$) in the stress-strain curve. (b), (c), (d) σ_l, σ_h and $\sigma_h - \sigma_l$ values of nanocrystalline NiTi with various average grain sizes as obtained from the present MD simulations (Fig. 7) and previous experiments [2–4].

temperature and the hardening in the stress-strain response. The occurrence of the single broad peak in the diffraction profiles of smaller grain sized cells after the martensitic transformation can be explained by the gradual evolution of lattice strain in the transformed structure caused by the severe constraint in small grains. A further decrease in the temperature or increase of the loading results in the growth of the martensite phase towards the grain boundaries. The resultant transformation strain is stored near the grain boundaries. The martensite-to-austenite transformation is a process to recover the initial, strain-free shape of the grains that existed in the original as-cast austenite phase. During the transformation, the stored transformation strain leads to the nucleation of the austenite phase near the grain boundaries and the austenite phase grows towards the grains' interior accompanied by the dissipation of the strain. As the stored strain energy is greater in nanocrystalline NiTi with smaller grains, the nucleation and growth of the austenite phase occurs at a lower temperature or at a higher stress level.

The formation of martensite domain boundaries and their effect on the phase transformation can also be explained by the *strain*

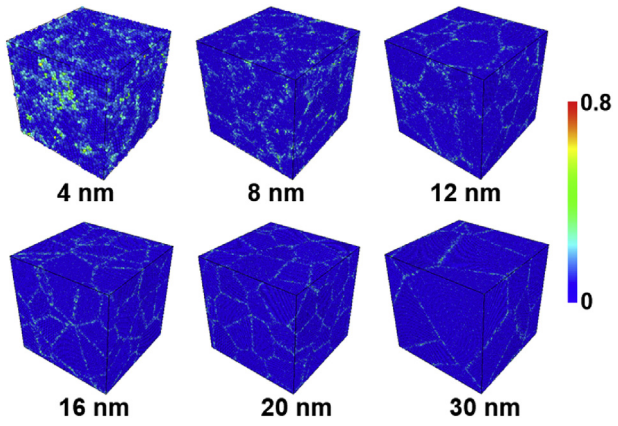

Fig. 13. Atomic configurations of nanocrystalline NiTi with various average grain sizes after the tensile loading and unloading processes at 400 K. The local shear strain [37] is visualized by different colors of atoms.

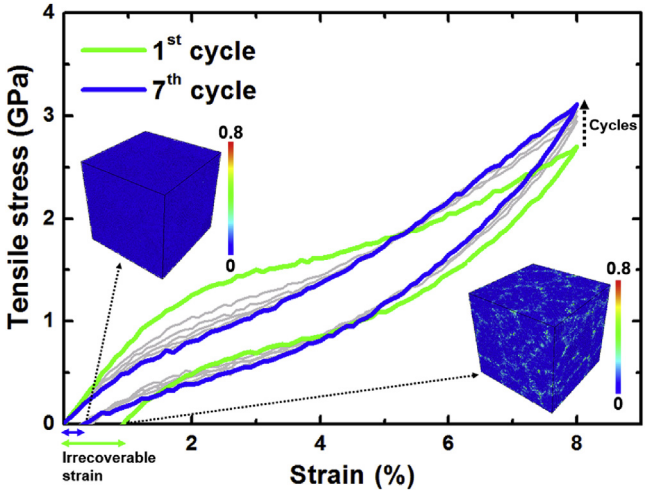

Fig. 14. Stress-strain response of nanocrystalline NiTi with an average grain size of 8 nm under tensile loading and unloading at 400 K. The response at the first and seventh cyclic loading are illustrated by the green and blue curves, respectively. The corresponding irrecoverable strain is emphasized by the green and blue arrows, and corresponding atomic configurations visualizing the local shear strain [37] are shown in the inset of the figure. The thin gray lines indicate the responses at intermediate (second – sixth) cyclic loadings. (For interpretation of the references to colour in this figure legend, the reader is referred to the web version of this article.)

contribution mechanism. Because the grain boundaries act as a mechanical constraint, the formation of a single martensite domain inside of a grain results in a highly localized strain near the grain boundaries. If the martensite phase inside of a grain forms with multiple domains, it can avoid the local accumulation of strain by the self-accommodation process [11,42]. Then, the transformation strain can be distributed to the domain boundaries as well as the grain boundaries. During the martensite-to-austenite transformation, the stored strain near the domain boundaries also leads to the nucleation of the austenite phase as shown by the present simulations (Figs. 6 and 11).

6. Summary and conclusions

Large-scale MD simulations have been performed to provide an atomic scale understanding of phase transformations in nanocrystalline NiTi shape-memory alloys. The present simulations faithfully reproduce the various experimentally reported characteristics of the phase transformations in nanocrystalline NiTi related to the over-stabilization of the austenite phase. The simulations further provide detailed insights into the atomic scale processes of the phase transformations. During the austenite-to-martensite transformation, the martensite phase nucleates in the grains' interior and grows towards grain boundaries. The resultant martensite phase is characterized by a unique nanotwinned structure with multiple domains. During the martensite-to-austenite transformation, the austenite phase nucleates at grain and domain boundaries and grows towards the grains' interior. In nanocrystalline NiTi with very small grains, a considerable amount of irrecoverable strain is observed during the stress-induced phase transformation. Our work clearly reveals that the irrecoverable strain results from a plastic deformation at the grain boundaries and that a pre-training under cyclic loading can greatly reduce this strain. By comprehensively analyzing experimental information and our results, a unified governing mechanism is proposed for the characteristics of both temperature- and stress-induced phase transformations in nanocrystalline NiTi. The strain contribution mechanism which focuses on the role of the grain boundaries as a mechanical constraint successfully explains observations of the present work as well as previous experiments. The present results provide a suitable theoretical basis to guide future design and applications of shape-memory alloys on the nanometer length scale.

Acknowledgements

Funding by the Deutsche Forschungsgemeinschaft (priority program SPP 1568), by the European Research Council (ERC) under the EU's 7th Framework Programme (FP7/2007-2013)/ERC (Grant No. 290998), and by the ERC under the EU's Horizon 2020 Research and Innovation Programme (Grant No. 639211) is gratefully acknowledged.

References

[1] K. Otsuka, X. Ren, Physical metallurgy of Ti–Ni-based shape memory alloys, Prog. Mater. Sci. 50 (2005) 511–678.
[2] A. Ahadi, Q. Sun, Stress hysteresis and temperature dependence of phase transition stress in nanostructured NiTi—Effects of grain size, Appl. Phys. Lett. 103 (2013) 021902.
[3] A. Ahadi, Q. Sun, Effects of grain size on the rate-dependent thermomechanical responses of nanostructured superelastic NiTi, Acta Mater. 76 (2014) 186–197.
[4] A. Ahadi, Q. Sun, Stress-induced nanoscale phase transition in superelastic NiTi by in situ X-ray diffraction, Acta Mater. 90 (2015) 272–281.
[5] A. Ahadi, Q. Sun, Grain size dependence of fracture toughness and crack-growth resistance of superelastic NiTi, Scr. Mater. 113 (2016) 171–175.
[6] K. Tsuchiya, M. Inuzuka, D. Tomus, A. Hosokawa, H. Nakayama, K. Morii, Y. Todaka, M. Umemoto, Martensitic transformation in nanostructured TiNi shape memory alloy formed via severe plastic deformation, Mater. Sci. Eng. A 438–440 (2006) 643–648.
[7] X. Shi, L. Cui, D. Jiang, C. Yu, F. Guo, M. Yu, Y. Ren, Y. Liu, Grain size effect on the R-phase transformation of nanocrystalline NiTi shape memory alloys, J. Mater. Sci. 49 (2014) 4643–4647.
[8] X.B. Shi, Z.Y. Ma, J.S. Zhang, H.L. Ding, F.M. Guo, Y. Liu, L.S. Cui, Grain size effect on the martensitic transformation temperatures of nanocrystalline NiTi alloy, Smart Mater. Struct. 24 (2015) 072001.
[9] T. Waitz, V. Kazykhanov, H.P. Karnthaler, Martensitic phase transformations in nanocrystalline NiTi studied by TEM, Acta Mater. 52 (2004) 137–147.
[10] T. Waitz, T. Antretter, F.D. Fischer, H.P. Karnthaler, Size effects on martensitic phase transformations in nanocrystalline NiTi shape memory alloys, Mater. Sci. Technol. 24 (2008) 934–940.
[11] T. Waitz, K. Tsuchiya, T. Antretter, F.D. Fischer, Phase transformations of Nanocrystalline martensitic materials, MRS Bull. 34 (2009) 814–821.
[12] W. Qin, Z.H. Chen, Stability of the austenitic phase in ultra-fine particles of Fe-based alloys, J. Alloys Compd. 322 (2001) 286–289.
[13] Q. Meng, N. Zhou, Y. Rong, S. Chen, T.Y. Hsu, Size effect on the Fe nanocrystalline phase transformation, Acta Mater. 50 (2002) 4563–4570.
[14] I.-W. Chen, Y.-H. Chiao, K. Tsuzaki, Statistics of martensitic nucleation, Acta Metall. 33 (1985) 1847–1859.
[15] R. Ahluwalia, S.S. Quek, D.T. Wu, Simulation of grain size effects in nanocrystalline shape memory alloys, J. Appl. Phys. 117 (2015) 244305.
[16] J. Schiøtz, F.D.D. Tolla, K.W. Jacobsen, Softening of nanocrystalline metals at

very small grain sizes, Nature 391 (1998) 561–563.
[17] J. Schiøtz, K.W. Jacobsen, A maximum in the strength of nanocrystalline copper, Science 301 (2003) 1357–1359.
[18] J.B. Jeon, B.-J. Lee, Y.W. Chang, Molecular dynamics simulation study of the effect of grain size on the deformation behavior of nanocrystalline body-centered cubic iron, Scr. Mater. 64 (2011) 494–497.
[19] Y.-F. Guo, Y.-S. Wang, W.-P. Wu, D.-L. Zhao, Atomistic simulation of martensitic phase transformation at the crack tip in B2 NiAl, Acta Mater. 55 (2007) 3891–3897.
[20] N. Lazarev, C. Abromeit, R. Schäublin, R. Gotthardt, Atomic-scale simulation of martensitic phase transformations in NiAl, Mater. Sci. Eng. A 481–482 (2008) 205–208.
[21] G.P. Pun, Y. Mishin, Molecular dynamics simulation of the martensitic phase transformation in NiAl alloys, J. Phys. Condens Matter 22 (2010) 395403.
[22] W.-S. Ko, B. Grabowski, J. Neugebauer, Development and application of a Ni-Ti interatomic potential with high predictive accuracy of the martensitic phase transition, Phys. Rev. B 92 (2015).
[23] K.R. Morrison, M.J. Cherukara, H. Kim, A. Strachan, Role of grain size on the martensitic transformation and ultra-fast superelasticity in shape memory alloys, Acta Mater. 95 (2015) 37–43.
[24] K.R. Morrison, M.J. Cherukara, K. Guda Vishnu, A. Strachan, Role of atomic variability and mechanical constraints on the martensitic phase transformation of a model disordered shape memory alloy via molecular dynamics, Acta Mater. 69 (2014) 30–36.
[25] B.-J. Lee, M.I. Baskes, Second nearest-neighbor modified embedded-atom-method potential, Phys. Rev. B 62 (2000) 8564–8567.
[26] B.-J. Lee, M.I. Baskes, H. Kim, Y. Koo Cho, Second nearest-neighbor modified embedded atom method potentials for bcc transition metals, Phys. Rev. B 64 (2001).
[27] B.-J. Lee, W.-S. Ko, H.-K. Kim, E.-H. Kim, The modified embedded-atom method interatomic potentials and recent progress in atomistic simulations, Calphad 34 (2010) 510–522.
[28] A.G. Frøseth, H. Van Swygenhoven, P.M. Derlet, Developing realistic grain boundary networks for use in molecular dynamics simulations, Acta Mater. 53 (2005) 4847–4856.
[29] S. Plimpton, Fast parallel algorithms for short-range molecular dynamics, J. Comput. Phys. 117 (1995) 1–19.
[30] S. Nose, A unified formulation of the constant temperature molecular dynamics methods, J. Chem. Phys. 81 (1984) 511.
[31] W.G. Hoover, Canonical dynamics: equilibrium phase-space distributions, Phys. Rev. A 31 (1985) 1695–1697.
[32] M. Parrinello, Polymorphic transitions in single crystals: a new molecular dynamics method, J. Appl. Phys. 52 (1981) 7182.
[33] C. Brandl, P.M. Derlet, H. Van Swygenhoven, Strain rates in molecular dynamics simulations of nanocrystalline metals, Philos. Mag. 89 (2009) 3465–3475.
[34] A. Stukowski, Structure identification methods for atomistic simulations of crystalline materials, Model. Simul. Mater. Sci. Eng. 20 (2012) 045021.
[35] J.D. Honeycutt, H.C. Andersen, Molecular dynamics study of melting and freezing of small Lennard-Jones clusters, J. Phys. Chem. 91 (1987) 4950–4963.
[36] A. Stukowski, Visualization and analysis of atomistic simulation data with OVITO–the open visualization tool, Model. Simul. Mater. Sci. Eng. 18 (2010) 015012.
[37] F. Shimizu, S. Ogata, J. Li, Theory of shear banding in metallic glasses and molecular dynamics calculations, Mater. Trans. 48 (2007) 2923–2927.
[38] S.P. Coleman, D.E. Spearot, L. Capolungo, Virtual diffraction analysis of Ni [0 1 0] symmetric tilt grain boundaries, Model. Simul. Mater. Sci. Eng. 21 (2013) 055020.
[39] S.P. Coleman, M.M. Sichani, D.E. Spearot, A computational algorithm to produce virtual X-ray and electron diffraction patterns from atomistic simulations, Jom 66 (2014) 408–416.
[40] Y. Kudoh, M. Tokonami, Crystal structure of the martensite in Ti-49.2 at.%Ni alloy analyzed by the single crystal X-ray diffraction method, Acta Metall. 33 (1985) 2049–2056.
[41] S.D. Prokoshkin, A.V. Korotitskiy, V. Brailovski, S. Turenne, I.Y. Khmelevskaya, I.B. Trubitsyna, On the lattice parameters of phases in binary Ti–Ni shape memory alloys, Acta Mater. 52 (2004) 4479–4492.
[42] T. Waitz, The self-accommodated morphology of martensite in nanocrystalline NiTi shape memory alloys, Acta Mater. 53 (2005) 2273–2283.
[43] D.C. Lagoudas (Ed.), Shape Memory Alloys, Springer, New York, 2008.
[44] J. Mohd Jani, M. Leary, A. Subic, M.A. Gibson, A review of shape memory alloy research, applications and opportunities, Mater. Des. 56 (2014) 1078–1113.